Multimode simulations of a wide FoV double-Fourier far-infrared spatio-spectral interferometer

Colm P. Bracken[a,b,*], John Lightfoot[c], Creidhe O'Sullivan[d], J. Anthony Murphy[d], Anthony Donohoe[d], Giorgio Savini[e], Roser Juanola-Parramon[f], On behalf of the FISICA Consortium

[a]*School of Physics, University College Dublin, Dublin, Ireland*
[b]*Astronomy & Astrophysics Section, Dublin Institute for Advanced Studies, Dublin 2, Ireland*
[c]*UK Astronomy Technology Centre, Edinburgh, Scotland, United Kingdom*
[d]*Department of Experimental Physics, Maynooth University, Kildare, Ireland*
[e]*Department of Physics and Astronomy, University College London, UK*
[f]*NASA Goddard Space Flight Centre, Greenbelt, Maryland, USA*

*Further author information:
C.P. Bracken: E-mail: cbracken@cp.dias.ie, Telephone: +353 85 715 1720

2017
SPIE Journal of Astronomical Telescopes, Instruments, and Systems

ABSTRACT

In the absence of 50 m class space-based observatories, sub-arc-second astronomy spanning the full far-infrared wavelength range will require space-based long-baseline interferometry. The long baselines of up to 10's of meteres are necessary to achieve sub arcsecond resolution demanded by the science goals. Also, practical observing times command a field of view toward an arc minute or so, not achievable with a single on-axis coherent detector. This paper is concerned with an application of an end-to-end instrument simulator PyFIInS, developed as part of the FISICA project under funding from the European Commission's 7th Framework Programme for Research and Technological Development (FP7). Predicted results of wide field of view spatio-spectral interferometry through simulations of a long-baseline, double-Fourier, far-infrared interferometer concept are presented and analysed. It is shown how such an interferometer, illuminated by a multimode detector can recover a large field of view at sub-arcsecond angular resolution, resulting in similar image quality as that achieved by illuminating the system with an array of coherent detectors. Through careful analysis, the importance of accounting for the correct number of higher-order optical modes is demonstrated, as well as accounting for both orthogonal polarisations. Given that it is very difficult to manufacture waveguide and feed structures at sub-mm wavelengths, the larger multimode design is recommended over the array of smaller single mode detectors. A brief note is provided in the conclusion of this paper, addressing a novel, more elegant solution to modelling far-infrared interferometers, which holds promise for improving the computational efficiency of the simulations presented here.

Keywords: Far-infrared FISICA interferometry double-Fourier PyFIInS (Python Far-Infrared Instrument Simulator) optics quasi-optics physical optics.

1. INTRODUCTION

1.1 FISICA (Far-Infrared Space Interferometer Critical Assessment)

With the cutting edge of space-based, far-infrared astronomy at somewhat of a halt, with the ESA Herschel Space Observatory[1,2] finished its mission, and the NASA Spitzer Space Telescope[3] now operating in its warm phase, we must now consider the next big leap in far-infrared astronomical observations. Although both Herschel and Spitzer operated successful missions with high spectral resolution, they were both limited in spatial resolution due to the fundamental diffraction limit of their 3.5 m and 0.85 m primary mirrors, respectively. Clearly then, high spatial resolution (sub-arc second) should be our next step in observing at these science-rich, but relatively long wavelengths. FISICA, a three year project that aimed to identify the scientific questions that can be answered with high spatial resolution far-infrared observations, and to translate these questions into a technological definition of a far-infrared space-based mission,[4,5] came to an end in December 2015. Funding for the FISICA study was under the European Commissions's FP7 programme.[6] The call for FP7 was open for seven years, for projects beginning in the years 2007 until 2013. The two main strategic objectives of FP7 were to strengthen the scientific and technological base of European industry, and to encourage its international competitiveness, while promoting research that supports EU policies.

FISICA built upon previous far-infrared interferometer studies carried out in Europe, such as the ESA Far-Infrared Interferometer (FIRI) Technology Reference Study (TRS).[7] Important work has also been going on in the U.S. over recent years, including the Space Infrared Interferometric Telescope (SPIRIT) study[8] (a candidate NASA Origins Probe mission), and the Balloon Experimental Twin Telescope for Infrared Interferometry (BETTII)[9] first launched in June 2017. The broad scope of the FISICA project in technologically defining a full mission, including a baseline optical design, required the collaboration of international researchers from a broad range of backgrounds, including leaders in the fields of far-infrared astronomy, cosmology, far-infrared instrumentation, optics, optical materials manufacture, and satellite positioning, among others.

1.2 FISICA baseline optical design

In a previous paper[10] a range of optical layouts were investigated toward identifying an optimal solution for the science requirements of the FISICA study. Table 1 summarises those science requirements,[4,11] and Table 2 details the parameters of the optimised optical layout.[10] Figure 1 shows a physical optics model of the system defined in Table 2.

The FISICA science case called for a wavelength range of $\lambda = 25 - 200$ μm, likely split into the three bands shown in Table 1. An extended wavelength range up to $\lambda = 400$ μm was also desirable for the science, but was deemed unfeasible due to the high level of diffraction, resulting in exceedingly large beams after propagation over the large baselines. Sensitivity requirements called for primary mirror diameters of 2 m. Figure 2 shows the response of a single primary mirror beam on the sky when illuminated by a single coherent detector horn, and Figure 3 shows the fringe pattern on the sky for two primary mirror sky beams for an interferometer at different baselines and wavelengths. Clearly, a single aperture lacks the sub-arc-second resolution defined by the FISICA science case. Furthermore, the beam for a single coherent detector is clearly too small to capture the full 1 arcmin squared FoV.

1.3 General approach to FISICA wide-FoV interferometric simulations

With a baseline design selected, and primary-mirror beams accurately modelled to show that the design can indeed satisfy the requirements of the FISICA science case whilst also minimising mass,[10] this paper is dedicated to simulating the system's performance as a wide FoV (field of view) interferometer. A system-level block diagram is shown in Figure 4. The previously modelled band 3 primary-mirror beams,[10] containing amplitude, phase, and polarisation information, are combined with a double-Fourier interferometer instrument simulator. The simulated beams, having been fully modelled from detector feed, through the hub condenser and primary condenser optics, contain the truncation and aberrations of realistic beams, except for aberrational effects due to mirror surface errors. Implementing these realistic beams in the simulator allows one to accurately assess the predicted response of an interferometer system in resolving point-like and near-point-like sources at various angular positions on the sky. More specifically, it is shown that if far-off-axis sources within the required 1' squared FoV are to be resolved, a single coherent detector will not be sufficient due to the limited FoV provided by a single detector beam. As such, a complete 3x3 array of detector beams are modelled for band 3 (100 - 200 μm), with the primary-mirror beam from each detector then fed-in to the Python simulator for simulation of source detection for that particular detector. By stacking the resulting simulated images, almost the full the 1' squared sky map can be reconstructed.

In addition to the detector array simulations, an alternative detector format is investigated and modelled. In place of an array of single-mode coherent detectors, one large multi-mode detector horn is modelled, with its independent modal beams then propagated through the optics of the interferometer system. The corresponding primary-mirror modal beams are then fed-in to the Python simulator, and it is shown that the full FoV can similarly be captured and resolved with this alternative approach. In a similar manner to how each coherent detector of an array must be modelled separately with the simulator, each of the TE (transverse electric) and TM (transverse magnetic) modes of a multi-mode detector must be modelled independently (including both polarisations of each mode). By subsequently stacking the images corresponding to each EM mode in post-processing, the complete 1' squared sky map can be reconstructed if a sufficient number of modes are allowed to propagate. The system is identical to the single-mode system, except for the focal plane, where one large horn is used in place of the nine single-mode horns.

The reason band 3 was the focus for simulation of the primary beams was due to diffraction and beam truncation effects being wavelength dependent, getting worse at longer wavelengths. In addition, generating vector beams becomes computationally demanding at shorter wavelengths. It would therefore be very challenging to simulate EM beams for bands 1 and 2 with a tool such as GRASP. Of course, the effects of aberration will be worse at shorter wavelengths, and the corresponding limitations on bands 1 and 2 are not considered in this paper. Previous work using ray tracing and Gaussian beam models has been reported,[12] where the effects of mirror surface form errors on interferometric visibility was analysed. The mirrors in the models presented in this paper are completely smooth. The aberrations are therefore purely a result of the geometry of the optics. Any additional aberrations arising from mirror surface roughness or mirror surface form errors would further effect visibility, and would thus need to be minimised in the manufacturing process.

Clearly, interferometry generally becomes more difficult at shorter wavelengths, simply due to the coherence length of light typically being proportional to wavelength. However, in the same manner that imaging properties are improved in a traditional (non-interferometer) system, additional optics can be employed in the design to reduce some of the frequency dependent aberration effects, and to improve interferometric visibility. Now, with

a traditional imaging system, in order to capitalise on the increased spatial resolution available at the higher frequencies of bands 1 and 2, one would need to increase the number of focal plane detectors to fulfil Nyquist sampling conditions. However, since the spatial resolution in an interferometer is due only to the baseline, Nyquist sampling on the focal plane is not relevant. However, to attain increased spectral resolution, a finer FTS step-size would be required. In terms of FoV for bands 1 and 2, a larger number of modes will simply propagate through to the detector in compensation for the narrowing beams at higher frequencies.

1.4 PyFIInS (Python Far-infrared Interferometer Instrument Simulator)

The simulator, PyFIInS,[13,14] is an end-to-end double-Fourier simulator that reads-in a sample sky model that should contain a number of point sources or extended sources, with each source having a defined spectrum. The input sky model file is created in '.fits' format, so it can be compatible with other astronomical image processing applications. PyFIInS then applies algorithms to the input sky model to simulate sampling the sky at a chosen number of u-v points with the two primary mirror beams, where one of the beams is modulated with a variable phase to simulate the delay line of an FTS (Fourier transform spectrometer). The result is a 3D data matrix (data-cube) containing the raw 2D data for the recorded intensity over the range of baselines $I(B, \phi)$, with a 1D interferogram $I(z)$ for each baseline, where B is the separation, or baseline between the two telescopes, ϕ is the angle of rotation of the two telescopes about the central hub, and z is the OPD (optical path difference) of the beam with the FTS delay line. The data reduction algorithms that are subsequently applied to the 3D data-cube output are called double-Fourier analysis,[15] since a Fourier transform must be applied to the u-v spatial data to resolve the sky sources in angular extent, as well as to the delay line data sets for each u-v point in order to spectrally resolve each source. The resulting double-Fourier-transformed data-cube is further reduced into spectral slices which represent images of the reproduced sky map at sample frequencies, as well as spectra at a defined range of points on the sky.

2. SIMULATING THE RESPONSE OF A 3×3 COHERENT DETECTOR ARRAY

2.1 Approach 1

In order to model the response of the 3×3 coherent detector array with PyFIInS, an input sky map with regularly distributed sources was chosen. A 5×5 grid of sources was defined, spanning -20 to +20 arc-seconds in both alt and az., at intervals of 10 arc-seconds. This regular grid of sources would allow the response of each separate detector beam to be more easily assessed, in a realistic observing scenario. Each of the 25 sources was given a Gaussian-like spatial profile with FWHM of approximately 2 arc-seconds, and a blackbody spectrum of temperature 10 K, where the full source parameters are shown in Table 3. The spatial and spectral profile of the model sky was combined into a 3D data-cude, for input into the PyFIInS simulations. Tables 4 and 5 in Appendix A describe some of the important simulated system values used in the model, where reasonable estimates were assumed in each case.

The telescope primary mirror field for each detector was generated separately using a physical optics modelling tool, GRASP, by Ticra.[16] The focal plane field of each of the nine detectors was represented by a single-moded rectangular horn aperture field. The horns were designed based on illuminating the primary mirror with an on-axis plane wave, allowing it to propagate through the optics and across the baseline, and then finding the best-fit Gaussian ($w = 0.77$ mm) to the resulting on-axis Airy pattern on the focal plane.[10] The central wavelength of the band (150 μm) was used for the design. The rectangular horn mouth that best couples to a Gaussian of radius $w = 0.77$ mm, and thus the plane wave, has a height of $b = 2w$ and a width of $a = \sqrt{2}b$.[10,17] The 3×3 array of horns were therefore given apertures of 2.18×1.54 mm, and were fed by rectangular waveguides with dimensions 0.11×0.055 mm.

The propagation of each horn aperture field was then simulated through the hub condensing optics, across the interferometric baseline, through the main telescope optics and condensers, and then recorded on a grid 10 cm in front of the telescope primary mirror. For each of the nine detectors a range of beams were in fact needed, as the beam profiles exhibited some dependence on baseline length, and of course the usual frequency-dependent beam narrowing (i.e. frequency-dependent gain). Beams for three baseline values were modelled for

each detector (5m, 50 m, and 100 m), and the PyFIInS simulator was programmed to interpolate appropriate beams for the remaining range of baselines of a given simulation based on the three input beams. PyFFInS was also programmed to apply appropriate scaling to the beams (in terms of their FWHM's) based upon the specific frequency values within the frequency band being simulated.

2.2 Results and discussion 1

Figure 5 (left) shows the results of a simulation for horn 1, corresponding to a detector at an off-axis position in both x and y on the array. Figure 5 (right) shows the results of a simulation for horn 5, corresponding to the on-axis detector. Figure 6 then shows the result of stacking the reproduced sky maps for all nine detector fields, with Figure 7 showing horizontal and vertical central cuts through the full sky images. As expected, all sources within the FoV are now detectable at $\lambda = 200$ μm, with the image showing a relatively decent SNR, although the signal from some sources near the limits of the FoV are not as strong as the on-axis source. This indicates some level of beam truncation for the off-axis pixels, which was in fact shown to be expected in the previous paper,[10] where the off-axis beams were shown to exhibit a small level of truncation for the longest baselines. This can of course be avoided if some of the optics are increased in size, such as the hub condensing optics, or the telescope primary mirror, for example. These increases will, in turn, clearly increase the mass of the system, which is not desirable.

The significant increase in overall intensity for the stacked image compared to the single-horn images is to be expected. There are two reasons for the significant increase after the stacking process is carried out for all nine horns. Each horn is sensitive to a number of sources (albeit not uniformly), so stacking the responses of each horn contributes more intensity to each source location. For example, the on-axis sky source in Figure 5 (right) detected by the central horn (horn 5) at an intensity of 1.4e-18, will actually partially couple to the beams of horns above, below, left, and right (2, 8, 4, 6, respectively), and less so to the horns on the corners of the array. In addition, Figure 5 shows only the response of one component of the E-field (E_x), whereas both E_x and E_y (analysed through the simulator separately) contribute intensity to the stacked image. The intensity contribution by E_y is less than E_x, as it is cross-polar power, but not insignificant for sources off boresight of a given horn.

The images at $\lambda = 100$ μm show a much poorer SNR in general, which is not surprising. Based on a blackbody temperature of 10 K, the intensity of the sources would be significantly weaker at 100 μm compared to 200 μm. The effects of aberration on interferometric visibility, which would be expected to be worse at higher frequencies, also likely contribute to the poorer images at 100 μm. This is supported by the significantly lower SNR for the off-axis sources, where beam aberration would be worse. A more advanced optical layout comprising a larger number of mirrors will likely be required for such a future system, in an effort to reduce aberration and increase interferometric visibility. In addition to the weaker emission of the 10 K sources and more severe aberration effects at $\lambda = 100$ μm, it is well understood that on-axis gain increases at shorter wavelengths at the expense of a narrower beam. As such, unless the off-axis coherent beams are exactly centred on an off-axis source, the TE_{11} mode beam at a higher frequency will generally be less sensitive to a given source. However, there is another, more subtle effect that essentially compensates for this beam-narrowing. As frequency is increased, higher-order modes will eventually begin to propagate and contribute to the beam, essentially re-widening the beam at the higher frequencies. Although only a single-mode was considered in this analysis, these subtle effects are analysed and discussed in section 3.2.

3. SIMULATING THE RESPONSE OF A PARTIALLY COHERENT, MULTI-MODE DETECTOR

3.1 Approach 2

As mentioned in the Introduction section, an alternative approach to filling the FoV, in place of an array of coherent detectors, is to use a single, partially coherent, multi-mode detector and feed horn. The aperture of this horn will of course be much larger than any of the horn apertures of the array, and the waveguide feed between the detector and horn must also be larger to allow the propagation of the higher-order modes. In the example modelled in this paper, the waveguide aperture was given dimensions of 0.34×0.17 mm, and it fed a

rectangular horn of dimensions 6.54×4.62 mm. The horn aperture field ($\vec{E_{ap}}$) resulting from the fundamental TE_{10} waveguide mode was then calculated, and propagated through the hub telescopes, across the interferometric baseline, and through the main telescopes. The resulting electric field components (E_x and E_y) were recorded on a Cartesian grid positioned 0.1 m from the sky-side of the main telescope primary mirrors, in the same manner to the approach used for the detector array primary beams. The primary beams corresponding to E_x and E_y were then used in separate simulations with PyFIInS, where the same 5×5 grid of sky sources was modelled. The same steps were repeated for the remaining higher-order TE and TM modes that could propagate through the waveguide and horn, the number of which was determined by the frequency being considered and the dimensions of the waveguide.

3.2 Results and discussion 2

Figure 8 shows the result of running the double-Fourier simulation of detecting the same 5×5 grid of sky sources as above, but with a primary mirror beam corresponding to illumination by the TE_{32} and TM_{21} modes of the multi-mode detector horn. Whereas each of the single-mode detectors of the array were sensitive to a specific source at a particular angular position on the sky, the higher order modes can often be sensitive to a number of sources, sometimes at opposite corners of the FoV. It is this property of an on-axis multi-mode detector that allows full detection of a larger FoV, provided enough modes are allowed to propagate.

Figure 9 then shows the result of stacking the images corresponding to a large number of modes. As with the array of single-mode horns, there is significant degradation in signal at the higher frequency, again primarily due to the 10 K blackbody intensity profile being weaker at 100 μm. However, there is another consideration that must be applied here. Given the full octave wavelength range within band 3, more modes can propagate at the shorter wavelength end of the band (100 μm), than at the longer end (200 μm). An example of the reception pattern on the sky for one of these high-frequency modes (TE_{13}) with cut-off wavelength lying within the wavelength span of band 3 is shown in Figure 10 (left). The corresponding TE_{13} simulated instrument response to the grid of sky sources is then shown in Figure 10 (right).

The result of including the higher order modes with cut-on wavelengths within the band 3 range is shown in Figure 11, with the single-mode array result shown again beside it for comparison. Once these extra modes are included, the SNR's at both ends of the band are very similar to the levels achieved with the detector array simulations, showing that the multi-mode detector approach is indeed roughly equivalent to using an array of coherent detectors. One reason why the multimode results at $\lambda = 100$ μm look slightly better than those of the single-mode detector array is likely due to a similar modal oversight as described above. The single-mode detectors will also exhibit some level of higher-order mode propagation at the shorter wavelengths of the band, but it will be much less significant than for the multimode detectors. This is illustrated in Figure 12, where the switch-on frequencies for the range of modes used are listed. When a waveguide is designed close to a given cut-off frequency, there will be roughly a doubling in frequency before any higher-order modes begin to propagate. As such, the TM_{01} and TE_{20}, which are just beginning to propagate at the highest frequencies of band 3 will likely add a very small amount of power to the sky response. Given the insignificant power likely contributed by this effect, no analysis was applied to it. In contrast to this, when a multimode horn/waveguide is designed to operate in a truly multimode nature, the number of propagating modes can increase by a factor of four for a given doubling of operational frequency.

4. CONCLUSIONS

As part of the three year FP7 FISICA study, a design for a long baseline ($B = 5 - 100$ m) far-infrared spatio-spectral double-Fourier interferometer concept was put forth. Since this baseline optical design is described in detail in other publications, so only a brief summary is outlined at the beginning of this paper. Using the chosen optical layout, realistic primary beams were generated using GRASP physical optics simulations. The resulting sky beams were then input to the PyFIInS instrument simulator in order to predict how the interferometer system would respond to a sky of small Gaussian sources distributed across the relatively large ≈ 1 acrmin squared field of view. Results of simulations from an array of single-mode detectors were compared to results from a larger on-axis multimode detector. Based on the presented simulated results, it was concluded that a single large multimode detector should provide Fourier-transformed interferometric images roughly equivalent

to using an array of single-mode detectors. In both cases the system performed well at the longer wavelengths ($\lambda \approx 200$ μm), but with significantly lower signal observed at ($\lambda \approx 100$ μm). This was to be expected given the blackbody intensity distribution of an array of 10 K sources being significantly weaker at the short end of the band.

It was also shown that one must take care with the number of optical modes to be modelled for a multimode detector. The much larger number of modes that can propagate at the higher-frequency end of a band can add significant power to the beam on the sky. This is particularly important for a waveband spanning a full octave (e.g. $100 - 200$ μm). A final note to be made, is that during the campaign of work described in this paper, an alternative simulation approach was brought to the attention of the authors. Based on the theoretical work of Withington et *al*,[18,19] a novel "black-box" approach considers the full far-infrared multiple-beam interferometer system as a kernel that transforms the sky map to the focal plane detector by means of a set of 'system modes', or eigenmodes of the entire system. The approach is novel and very efficient, and would allow much faster analysis of a FISICA-type system. This elegant solution will be the focus of future simulations in this area.

Acknowledgements

This research has received funding from the European Union's Seventh Framework Programme (FP7/2007 - 2013) under FISICA grant agreement no. 312818. The corresponding author also acknowledges Science Foundation Ireland (SFI) for financial assistance throughout the period of research, under SFI grant no. 15/IA/2880.

REFERENCES

[1] Servillat, M., Coleiro, A., Chaty, S., Rahoui, F., and Zurita-Heras, J., "Herschel observations of dust around the high-mass x-ray binary gx 301-2," *The Astrophysical Journal* **797**(2), id. 114, 10 pp (2014).

[2] Oteo, I., "Dust correction factors over 0<z<3 in massive star-forming galaxies derived from a stacking analysis of herschel data," *Astronomy and Astrophysics* **572**, id. L4, 12 pp (2014).

[3] Werner, M., Fazio, G., Rieke, G., Roellig, T., and Watson, D., "First fruits of the spitzer space telescope: galactic and solar system studies," *Annual Review of Astronomy and Astrophysics* **44**(1), 269–321 (2006).

[4] Savini, G., Ade, P., Baccichet, N., Bracken, C., and et al., "Progress in the critical assessment for a far-infrared space interferometer with double fourier modulation (FP7-FISICA)," *OSA Technical Digest, Optical Society of America* **Imaging FTS in Astronomy (FT4A)**, FT4A.3 (2015).

[5] Iafolla, V., Fiorenza, E., Iafolla, L., Lefevre, C., Magnafico, C., Santoli, F., and Spinoglio, L., "FISICA (far infrared space interferometer critical assessment) metrological problems and system requirements for interferometric observations from space," *Proceedings of IEEE* **Metrology for Aerospace (MetroAeroSpace)**, 161–166 (2014).

[6] "FP7." https://ec.europa.eu/research/fp7/understanding/fp7inbrief/what-is$_e$n.*html*.

[7] Helmich, F. and Ivison, R., "FIRI - a far-infrared interferometer," *Experimental Astronomy* **23**(1), 245–276 (2009).

[8] Leisawitz, D. and et al., "The space infrared interferometric telescope (SPIRIT): High-resolution imaging and spectroscopy in the far-infrared," *Journal for Advanced Space Research* **40**(1), 689–703 (2007).

[9] Rinehart, S. and et al., "The balloon experimental twin telescope for infrared interferometry (BETTII): An experiment for high angular resolution in the far-infrared," *Publications of the Astronomical Society of the Pacific* **126,**(941), 660–673 (2014).

[10] Bracken, C., O'Sullivan, C., Murphy, J. A., Donohoe, A., Savini, G., Lightfoot, J., and Juanola-Parramon, R., "Quasi-optical analysis of a far-infrared spatio-spectral space interferometer concept," *Infrared Physics and Technology* **77**, 171–178 (July 2016).

[11] Spinoglio, L., Schito, D., Pezzuto, S., Holland, W., and on behalf of the FP7-FISICA Consortium, "D1.1: Definition/update of key science questions and relevant data products," *FP7-FISICA Consortium* (2014).

[12] Bracken, C. and on behalf of the FP7-FISICA Consortium, "Optical and quasi-optical analysis of system components for a far-infrared space interferometer," *Proceedings of SPIE 9362* **Terahertz, RF, Millimeter, and Submillimeter-Wave Technology and Applications VIII**(93620N), 12 pp. (2015).

[13] Juanola-Parramon, R., *A far-infrared spectro-spatial space interferometer. Instrument simulator and testbed implementation*, PhD thesis, UCL (University College London) (2014). PhD Thesis.

[14] Lightfoot, J., Juanola-Parramon, R., and Savini, G., "FIInS - a python simulator for a far-infrared double fourier interferometer in space," *OSA Technical Digest, Optical Society of America* **Hyperspectral Imaging and Sounding of the Environment (JM3A)**, JM3A.9 (2015).

[15] Elias-II, N., Harwit, N., Leisawitz, D., and Rinehart, S., "The mathematics of double-Fourier interferometers," *The Astrophysical Journal* **657**(2), 1178–1200 (2007).

[16] Pontoppidan, K., "GRASP technical description," *TICRA* (2008).

[17] Murphy, J. A., Padman, R., and Hills, R., "An experimental submillimetre heterodyne array receiver," *International Journal of Infrared and Millimeter Waves* **9**(4), 325–350 (1988).

[18] Withington, S., Hobson, M., and Campbell, E., "Modal analysis of astronomical bolometric interferometers," *Journal of the Optical Society of America. A* **21**, 1988–1995 (Oct 2004).

[19] Saklatvala, G., Hobson, M., and Withington, S., "Simulations of multimode bolometric interferometers," *Monthly Notices of the Royal Astronomical Society* **367**, 1194–1200 (2006).

Colm Bracken is a post doctoral research fellow at the Dublin Institute for Advanced Studies (DIAS), in the Astronomy Astrophysics section of the School of Cosmic Physics. He received his BSc and PhD degrees in physics with astrophysics at National University of Ireland, Maynooth in 2010 and 2015, respectively. He is the author of a number of journal papers on electromagnetic analysis and design of receivers and detectors for far-infrared astronomy and interferometry. His current research interests include large-format arrays of Microwave Kinetic Inductance Detectors (MKIDs) for optical/near-infrared wavelengths, and microwave readout systems for MKIDs.

Biographies and photographs of the other authors are not available.

Parameter	Desired	Requirement
Field of View (θ, ϕ)	1' × 1'	Multiple Detectors/Modes
Angular Resolution	$\Delta\theta_{min} < 0.1''$	$B_{max} \approx 100$ m (for longest λ's)
Waveband 1	$\Delta_\lambda = 25 - 50$ μm	$\Delta_\nu = 6 - 12$ THz, $\Delta_k = 200 - 400$ cm^{-1}
Waveband 2	$\Delta_\lambda = 50 - 100$ μm	$\Delta_\nu = 3 - 6$ THz, $\Delta_k = 100 - 200$ cm^{-1}
Waveband 3	$\Delta_\lambda = 100 - 200$ μm	$\Delta_\nu = 1.5 - 3$ THz, $\Delta_k = 50 - 100$ cm^{-1}

Table 1. Requirements of the interferometer system, driven by the FISICA science requirements.[11]

Primary Telescopes (Cassegrain afocal)	Focal Length [m]	De-magnification (f_1/f_2)	Mirror Radius [m]	$F/\#$	Conic Const.
Primary (M1)	3	10	1	1.5	-1
Secondary (M2)	0.3		0.1	1.5	-1
Hub Condensers (Gregorian afocal)	Focal Length [m]	De-magnification (f_3/f_4)	Mirror Radius [m]	$F/\#$	Conic Const.
Primary (M3)	0.2	5	0.20	0.5	-1
Secondary (M4)	0.04		0.043	0.465	-1

Table 2. Parameters of both the light collecting telescopes and hub condensers.

Source Number [#]	1	2	n	25
Position (Alt/Az) [arcsecs]	-20/+20	-10/+20	.....	+20/-20
Intensity Profile	Gaussian	Gaussian	.....	Gaussian
Extent (FWHM) [arcsecs]	2	2	.....	2
Temperature [K]	10	10	.....	10
Spectrum (Continuum)	Blackbody	Blackbody	.....	Blackbody
Spectrum (Lines)	0	0	.....	0
Opacity Dependence [β]	0	0	.....	0
Peak Flux [Jy]	1	1	.....	1

Table 3. Full parameters for the array of sky sources. The absolute fluxes were not considered important for the work. The relative fluxes, each normalised to have on-axis intensity of 1 Jansky, were kept constant for each simulation presented throughout the paper.

Telescopes	Parameter	Value
	Primary mirror diameter	2 m
	Mirror temperature	4 K
	Telescope emissivity	0.05
	Number of mirrors in telescopes	3
FTS	Parameter	Value
	Wavenumber Min. (λ_{max})	50 cm^{-1} (200 μm)
	Wavenumber Max. (λ_{min})	100 cm^{-1} (100 μm)
	Points per Nyquist	1
	Spectral resolution	$R = 100$
	V (Drive)	1.5 cm/s
	Number of scans	4
	Interscan delay	0.1 s
	V (Error type)	Herschel
Detectors	Parameter	Value
	Detector time constant	$\tau = 200$ μs
	Detector optical absorption efficiency	0.57
	Number of detector modes	1
	No. time constants per acquisition	n = 1
	Acquisiton frequency $1/(n\tau)$	5000 Hz
	Knee frequency	0.1 Hz
	Cosmic rays	0

Table 4. Parameters and settings of the telescope and interferometer system, as used in the simulations throughout this paper.

Cold Optics	Parameter	Value
	Optical efficiency	0.3
	Number of mirrors (L)	4
	Cold optics box temperature	2 K
	Instrument emissivity	0.7
	Cold optics mirror emissivity	0.05
	Dichroic transmission	0.98
	Dichroic reflectivity	0.98
	Combiner transmission	0.487
	Combiner reflectivity	0.487
	Window efficiency	0.98
	NIRFIR dichroic Tx	0.98
	Filter Tx	0.98
	Number of mirrors (R)	5
Warm Optics	Parameter	Value
	BSM temperature	4 K
	BSM emissivity	0.05
	K-mirror temperature	4 K
	K-mirror emissivity	0.05
	Number of mirrors in K-mirror	3
Background	Parameter	Value
	CMB temp	2.726 K
	CIB temp	20 K
	CIB emissivity @ 200um	1.30E-05
	Zodi dust temp	220 K
	Zodi emissivity @ 30um	7.00E-08
	Solar temp	5800 K
	Zodi scattering coeff	5.00E-14
	Stray light temperature	70 K
	Stray light coefficient	1.00E-06

Table 5. Reasonably sensible values for efficiency, emissivity, noise, etc., as used in the simulations throughout this paper.

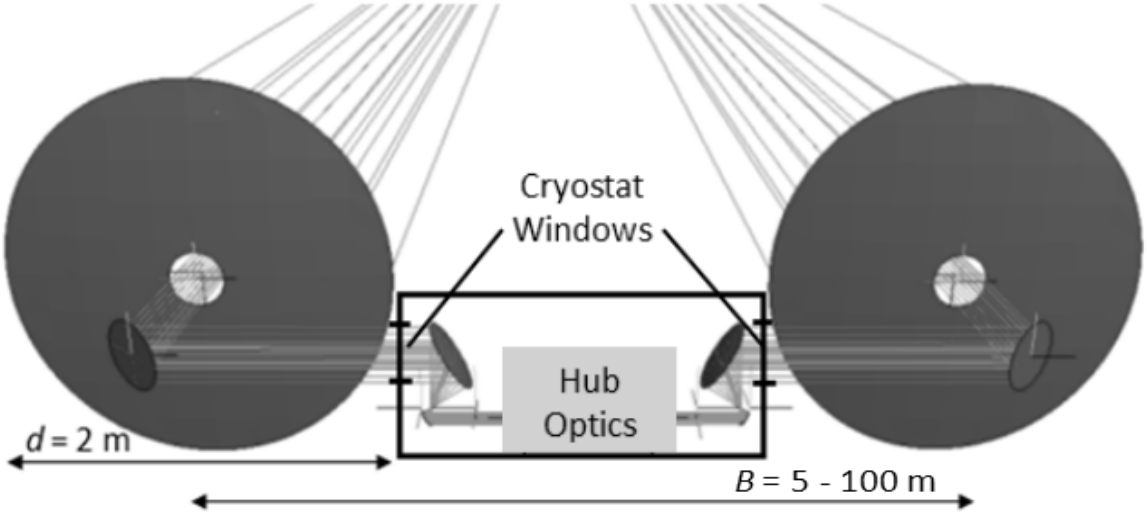

Figure 1. Interferometer concept design, generated using GRASP PO software[16]

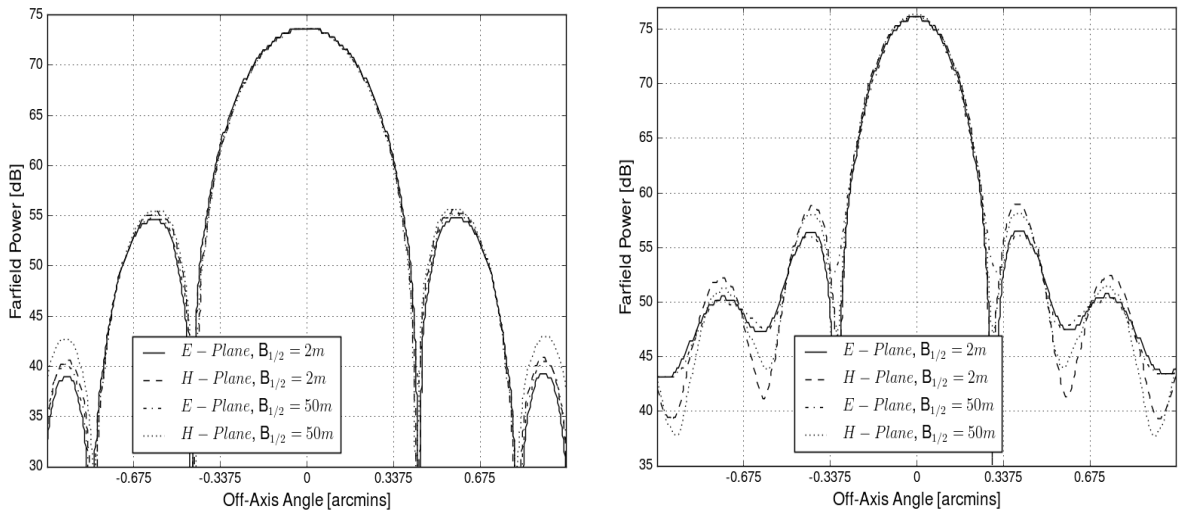

Figure 2. *Left*: Far-field patterns for a single telescope illuminated by an on-axis feed horn at a wavelength of $\lambda = 200$ μm, and *Right*: $\lambda = 100$

.

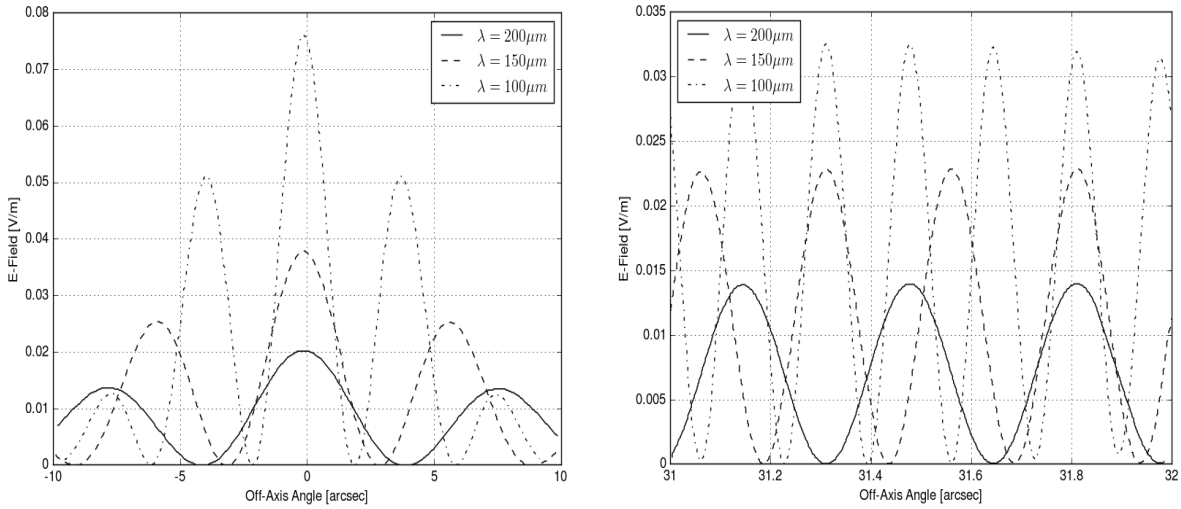

Figure 3. *Left*: Cuts through far-field interferometric beam pattern for two 2 m telescopes illuminated by an on-axis single-mode horn antenna and a baseline of $B = 5$ m, giving resolutions of $\theta = 4''$ at $\lambda = 100$ μm, and $\theta = 8''$ at $\lambda = 200$ μm. *Right*: Cuts through interferometric beam pattern for an off-axis single-mode horn antenna and a baseline of $B = 50$ m, giving resolutions of $\theta = 0.4''$ at 100 μm, and $\theta = 0.8''$ at 200 μm, as would be expected. The amplitude (E) being lower the longer wavelength is to be expected, as the gain ($\log(E^2)$) of each primary beam is lower at the longer wavelength.

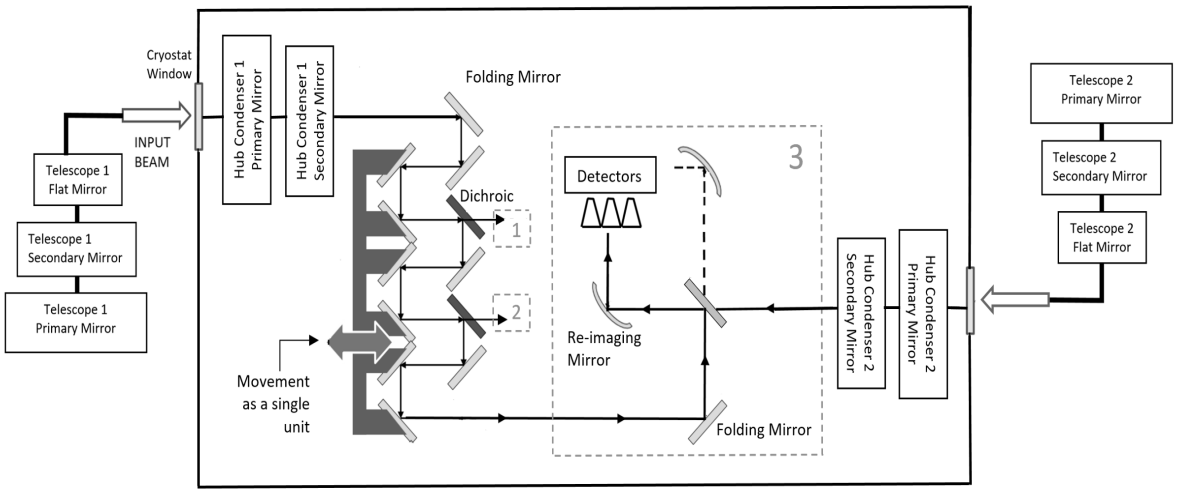

Figure 4. Block diagram for the optical path of the FISICA concept instrument, showing all of the main optical elements and the band 3 beam combiner and re-imaging mirrors. The array of single mode horns is visible. The multimode system is identical, except for the array of small horns replaced by one larger horn. This design allows the beam that exits at final stage to have travelled over an OPD (optical path difference) twice as large as the frequencies that exit at the second stage, which themselves will have travelled an OPD twice that of the first pass-band. This is ideal, given that the required FTS OPD sample size for Band 1 is twice that of Band 2, which itself is twice that of Band three.

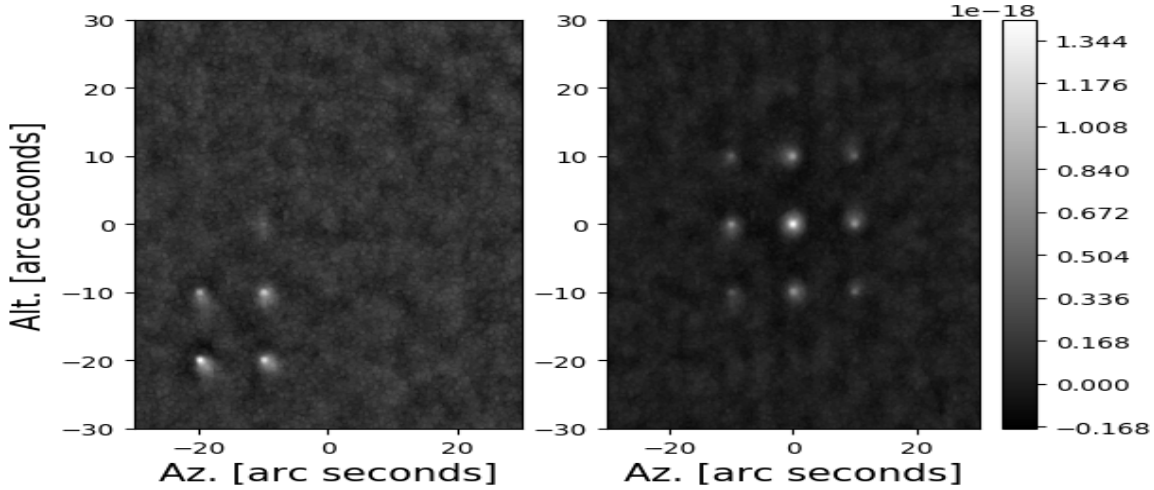

Figure 5. *Left*: Reconstructed sky map at $\lambda = 200$ μm for PyFIInS simulation of the 5×5 grid of sources, using detector 1 (corner pixel in 3×3 pixel array). *Right*: Reconstructed sky map at $\lambda = 200$ μm, using detector 5 (central pixel in 3×3 array).

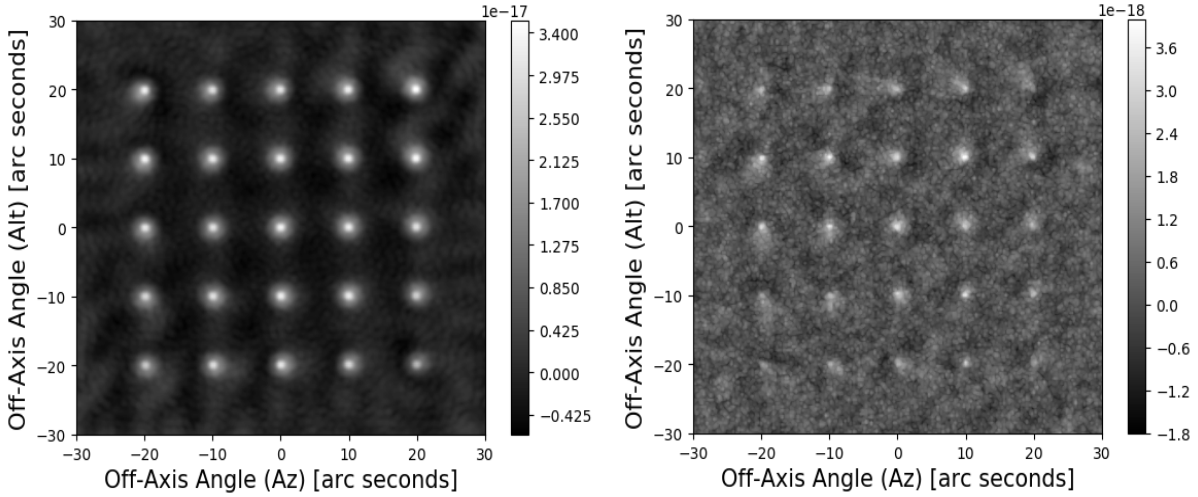

Figure 6. *Left*: Full reconstructed sky map at $\lambda = 200$ μm for combined PyFIInS simulations of the 5×5 grid of sources, using all nine detectors of the 3×3 pixel array. *Right*: Full reconstructed sky at $\lambda = 100$ μm. Each detector was simulated separately with PyFIInS. The resulting sky maps stacked in post-processing.

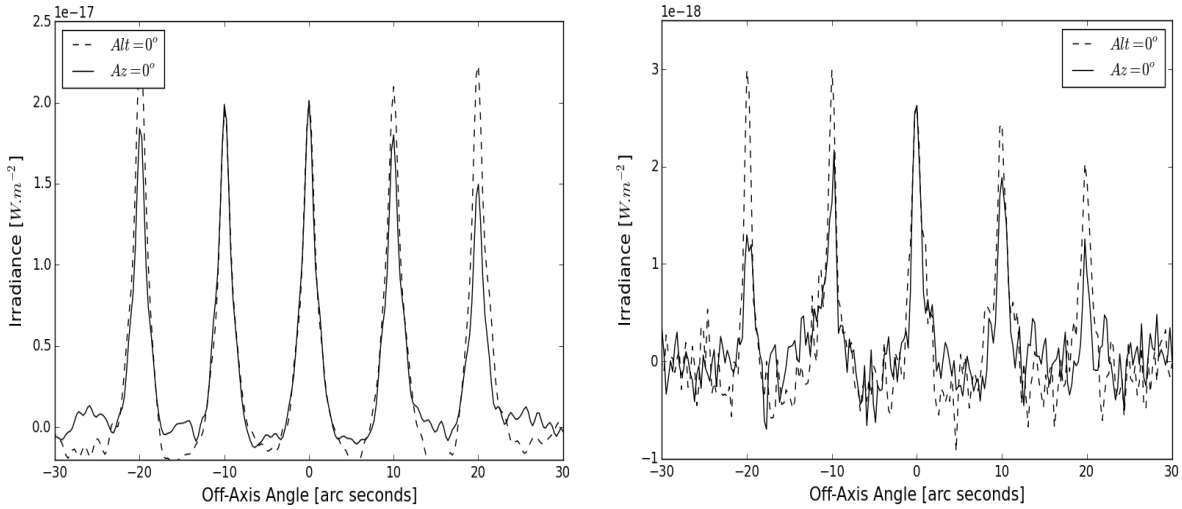

Figure 7. *Left*: Horizontal and vertical cuts through centre of reconstructed sky map (Figure 6, left) at $\lambda = 200$ μm. *Right*: Horizontal and vertical cuts through centre of reconstructed sky map (Figure 6, right) at $\lambda = 100$ μm.

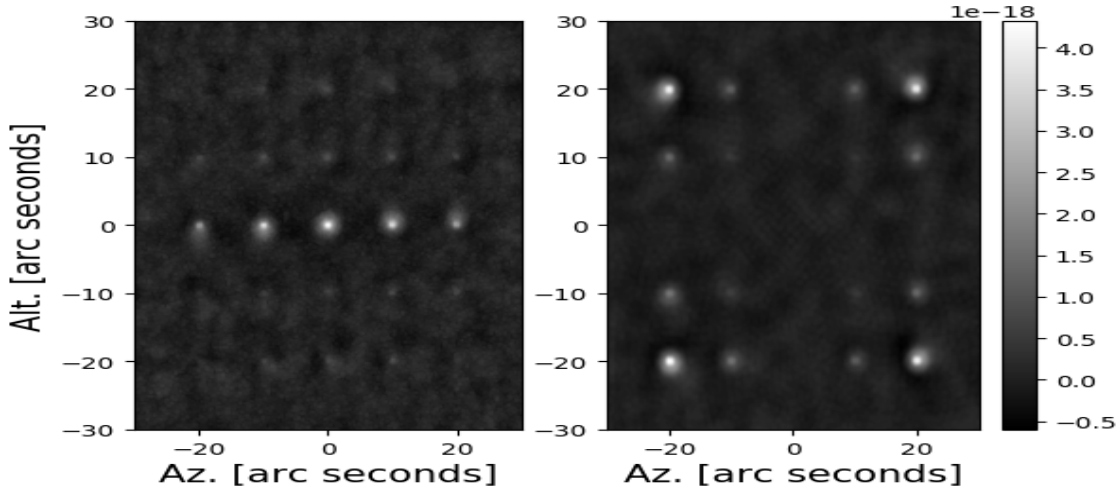

Figure 8. *Left*: Reconstructed sky map at $\lambda = 100$ μm for PyFIInS simulation of the 5×5 grid of sources, using the x-component (E_x) of mode TE_{32} of the multi-mode detector horn. *Right*: Reconstructed sky map at $\lambda = 200$ μm, using the y-component (E_y) of mode TM_{21} of the multi-mode detector horn.

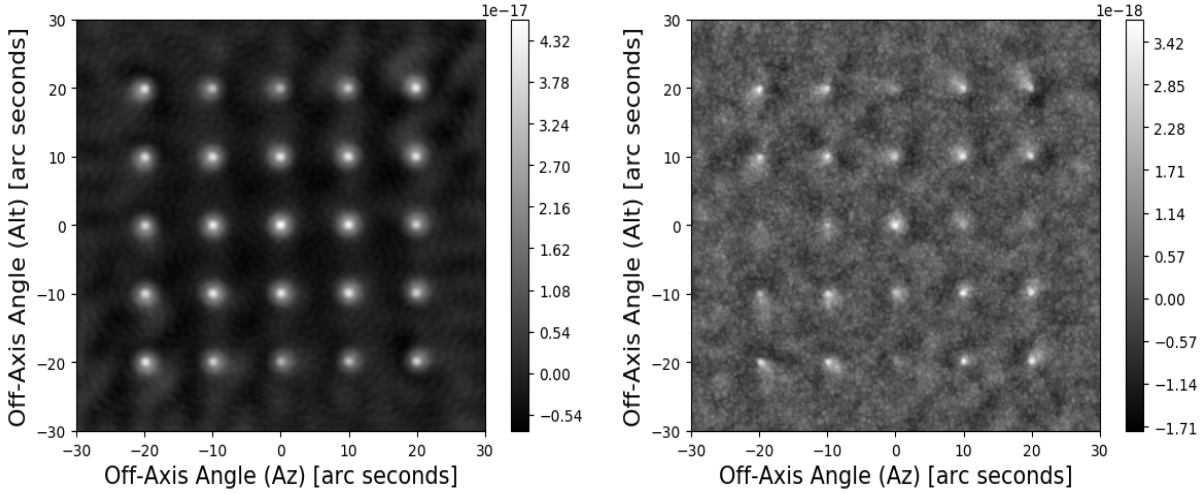

Figure 9. *Left*: Reconstructed sky map at $\lambda = 200$ μm for PyFIInS simulation of the 5×5 grid of sources, using the x and y components of a large number of TE and TM modes of the multi-mode detector horn. *Right*: Reconstructed sky map at $\lambda = 100$ μm, using the same modes.

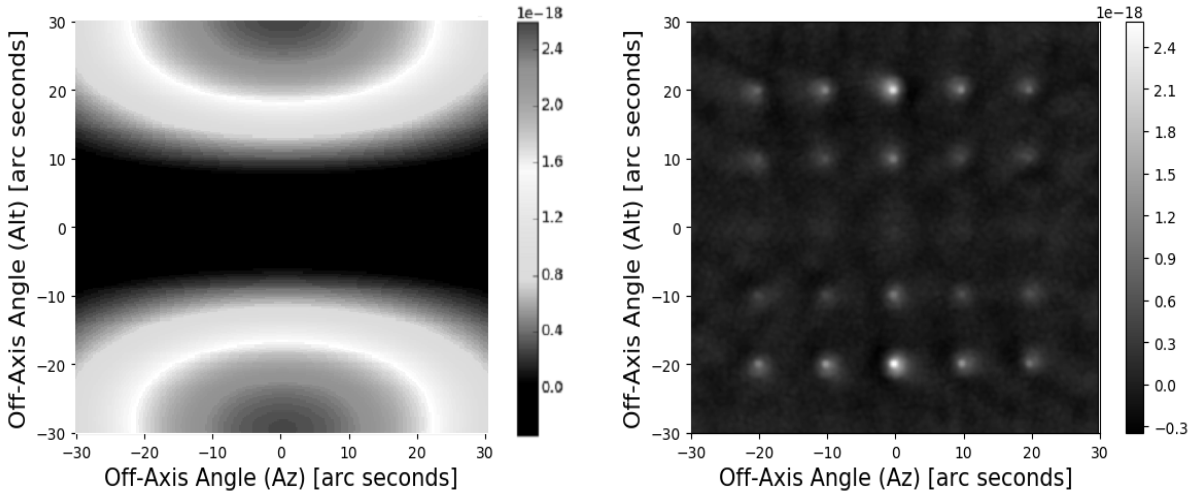

Figure 10. *Left*: TE_{13} mode (x-component) beam response on the sky, and *Right*: TE_{13} mode detection of model sky, for $\lambda = 100$ μm.

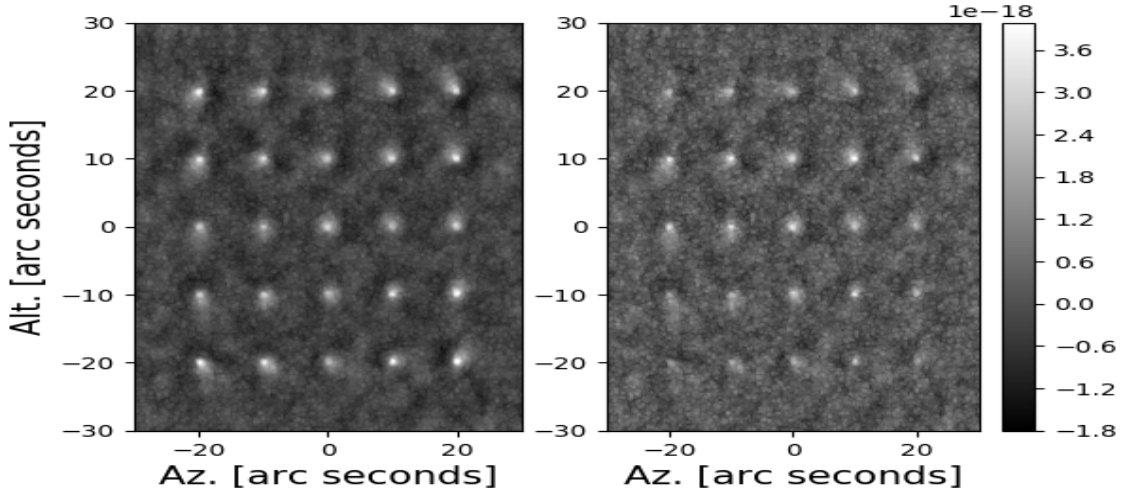

Figure 11. *Left*: Reconstructed sky map at $\lambda = 100$ μm for PyFIInS simulation of the 5×5 grid of sources, using the x and y components of a large number of TE and TM modes of the multi-mode detector horn, including the additional modes that can propagate only at higher frequencies. *Right*: Reconstructed sky map at $\lambda = 100$ μm, using the array of single-mode detectors.

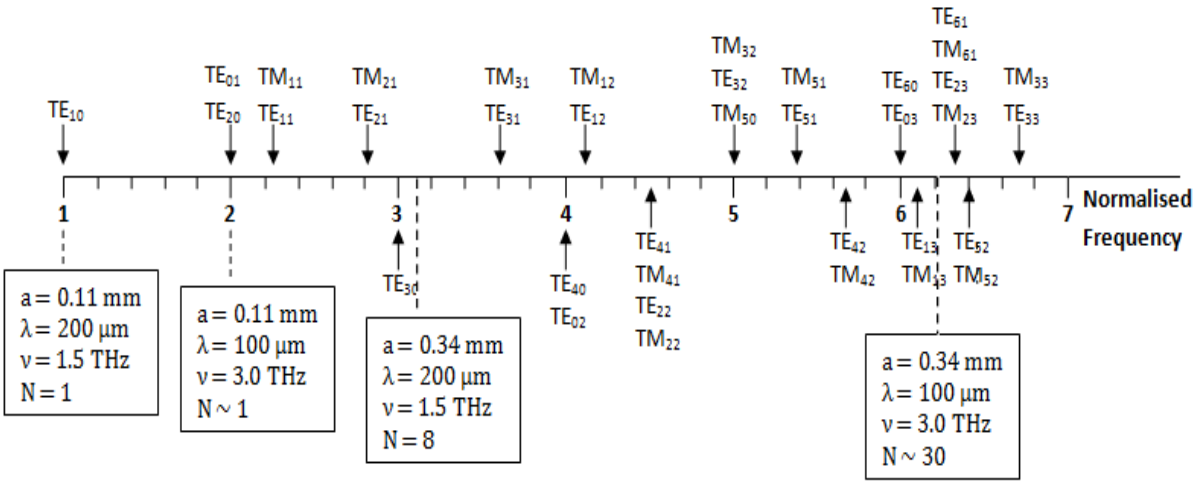

Figure 12. Switch on frequencies for a horn fed by a single-mode waveguide ($a = 0.11$ mm), and the number of propagating modes possible for both the single-mode waveguide, as well as a multimode horn and waveguide ($a = 0.34$ mm) at either end of band 3. The frequency scale is normalised to the cut-off frequency of the single-mode waveguide. In both cases N is the number of propagating modes.